TITLE
Improved sample dispersion in cryo-EM using "perpetually-hydrated" graphene oxide flakes

ARTICLE TYPE
Technical report

AUTHORS/AFFILIATIONS
Martin Cheung[1]*†, Hidehito Adaniya[1†], Cathal Cassidy[1], Masao Yamashita[1], Kun-Lung Li[1], Seita Taba[1], and Tsumoru Shintake[1]

[1]Quantum Wave Microscopy Unit, Okinawa Institute of Science and Technology Graduate University, Kunigami District, Okinawa Prefecture, Japan, 904-0412

*Correspondence: martin.cheung@oist.jp

† These authors contributed equally to this work

Key words: cryo-electron microscopy; vitreous ice; sample preparation; vitrification

MAIN TEXT

Abstract

For many macromolecular complexes, the inability to uniformly disperse solubilized specimen particles within vitreous ice films precludes their analysis by cryo-electron microscopy (cryo-EM). Here, we introduce a sample preparation process using "perpetually-hydrated" graphene oxide flakes as particle support films, and report vastly improved specimen dispersion. The new method introduced in this study incorporates hydrated graphene oxide flakes into a standard sample preparation regime, without the need for additional tools or devices, making it a cost-effective and easily adoptable alternative to currently available sample preparation approaches.

1. Introduction

Achieving uniform particle dispersion in the thinnest ice permissible by the specimen is a fundamental requirement of the cryo-electron microscopy (cryo-EM) approach (Dubochet et al, 1988; Frank, 2006; Orlova and Saibil, 2011). Whilst cryo-EM has seen tremendous technological advances in recent years, a persistent problem is that many macromolecular complexes (e.g. viruses, multimeric protein assemblies) resist uniform dispersion within vitreous ice films spanning holes of an amorphous carbon support. The biconcave nature of unsupported nanometer-thick ice films, coupled with adhesion between specimen particles and the amorphous carbon support, cause particle agglomeration at the peripheries of holes thus preventing uniform particle dispersion (**Fig. S1a**) (Burrows and Penn, 2013). In severe cases, poor particle dispersion can preclude the application of cryo-EM to certain specimens.

To surmount this issue, various grid treatment, blotting and sample application methods have been proposed (Lu et al., 2009; Cheung et al., 2013; Meyerson et al., 2014; Razinkov et al., 2016; Arnold et al., 2016; Snijder et al., 2017). A particularly promising solution involves the use of sub-nanometer thick carbon films, such as graphene or graphene oxide (GO), mounted atop the amorphous carbon support as an additional sample support film. Such supports can potentially improve particle dispersion by providing a surface for particles to adsorb to during sample preparation (**Fig. S1b**), with minimal loss of image contrast via electron scattering (Pantelic et al., 2010; Pentelic et al., 2011). Whilst graphene is not water soluble or solution-processable, as-synthesized GO is intrinsically hydrophilic and can be readily solubilized in water and polar aprotic solvents (Paredes et al., 2008; Neklyudov et al., 2017). Furthermore, the numerous oxygen-containing functional groups located in the sp3-hybridised domains facilitate binding to organic materials through non-covalent, covalent and/or ionic interactions (Loh et al., 2011). These qualities have led to much interest in utilizing GO in cryo-EM (Pantelic et al., 2010; Yuan et al., 2011; Patterson et al., 2012).

Reports utilizing graphene or GO in cryo-EM studies have typically employed commercial or self-prepared air-dried graphene/GO film grids. Due to the temporal adsorption of organic contaminants to these films under desiccating conditions, surface charges are gradually diminished, eventually rendering them hydrophobic (Dubochet et al., 1982; Russo and Passmore., 2014). This loss of hydrophilicity severely inhibits successful particle adsorption, dispersion and can result in surface dewetting, which manifests as vitreous ice film discontinuity in cryo-EM (**Fig. S2**) (van de Put et al., 2015). While various graphene/GO film pre-treatment processes have been proposed to prevent dewetting and improve particle dispersion, in general, they consistently seek to reverse or compensate for changes in charge states and the loss of hydrophilicity (Russo and Passmore., 2014; van de Put et al., 2015).

We hypothesized that particle adsorption to GO and thus dispersion could be ameliorated if this drying-related loss of hydrophilicity were avoided altogether by keeping the GO hydrated at all times. Based on this, we propose an alternative method that utilizes "perpetually-hydrated" GO flakes (hereinafter termed 'hydrated-GO process') to improve particle dispersion in vitreous ice films for a selection of macromolecular complexes.

2. Grid preparatory methods tested

Hydrated-graphene oxide process. Quantifoil R3.5/1 holey amorphous carbon films mounted on 200 mesh gold grids (Quantifoil Micro Tools GmbH) were hydrophilised by plasma treatment of the carbon side only for 2 x 60 s (120 s total) in an Electron Microscopic Hydrophilic Processor (DII - 29020HD, JEOL), with the amorphous carbon support facing the plasma source. Plasma treatment was typically conducted an hour before use and grids were stored in a desiccator until required.

Hydrophilised grids were tweezed on the outer rim, with minimal intrusion into the grid, using Vitrobot-compatible tweezers (G3, Mel-Build) and placed inside the chamber of a Vitrobot Mark IV (FEI). Chamber settings were set at 4 °C and 100% humidity. Filter paper (#597, Whatman) was placed on both blotting pads approximately 30 min – 1 hr before blotting.

Hydrated graphene oxide flake dispersion at 2 mg/ml concentration (Sigma Aldrich, Cat: 763705-25ML) was diluted 1/10 in Milli-Q water to a working concentration of 0.2 mg/ml. This dilution was typically done on the day of the experiment and kept at room temperature

until required. A 3 µl drop of the diluted suspension was pipetted onto the amorphous carbon support of the grid in the Vitrobot chamber and allowed to incubate for 50 s. Following this, 3 µl of sample was pipetted onto the opposite, non-carbon face of the grid. Double-sided blotting was commenced immediately using a single blotting motion of blot force 2, blot time of 1 s and drain time of 1 s, followed by immediate plunge-freezing into liquid ethane. In total, the diluted graphene oxide flake dispersion was incubated with the grid for ~60 s before commencement of blotting (50 s initial incubation period plus ~10 s when the sample was being applied).

Conventional vitrification process for unsupported vitreous ice films and air-dried graphene oxide film grids. The conventional vitrification process followed the same steps as the hydrated-GO process, as detailed above, except that no graphene oxide incubation step was implemented. Instead, 3 µl of sample solution was applied directly to either the hydrophilised amorphous carbon support of a Quantifoil R3.5/1 grid (for unsupported vitreous ice films) or the graphene oxide face of an air-dried graphene oxide film grid (see Air-dried graphene oxide film grid fabrication) inside the Vitrobot chamber. Blotting conditions were the same as those used for the hydrated-GO process.

Air-dried graphene oxide film grid fabrication. 3 µl of diluted (0.2 mg/ml) graphene oxide solution was applied to the hydrophilised amorphous carbon support of a Quantifoil R3.5/1 grid. The grid was incubated at room temperature for 40 s before excess liquid was removed by blotting with Whatman #597 filter paper. The grid was allowed to dry in a desiccator for 1 hr at room temperature. Fully dried graphene oxide film grids were then used in the conventional vitrification process, as described above.

3. Electron microscopy and cryo-electron microscopy

Imaging of all grid preparations in this study was conducted using a prototype low-kV cryo-electron microscope (DMF4000) with scanning electron microscopy (SEM), scanning transmission electron microscopy (STEM), diffraction, TEM and in-line electron holographic imaging capabilities, currently being developed at the Okinawa Institute of Science and Technology Graduate University (OIST, Japan), specific details of which can be found in Adaniya et al., 2018. All imaging was performed at 20 kV as this permits high-contrast imaging of ice-embedded particles and easier assessment of ice thickness variations.

All cryo-electron microscopy imaging was conducted when the measured holder temperature was between -175 °C and -180 °C. To visualize graphene oxide distribution across the entire grid surface, low-magnification images were acquired in either SEM or STEM mode. For imaging of individual holes, the microscope was operated in TEM mode, with point projection illumination conditions and with the grid situated 100 µm downstream from the electron beam convergence point. All images were acquired with an exposure time of 500 ms, which equated to a cumulative dose of 2 $e^-/Å^2$ on the sample. Images were recorded on an 8,000 x 8,000 pixel charged couple device (CCD) detector (TVIPS), with 4x binning applied to improve signal-to-noise.

To confirm the presence of vitrified graphene oxide flakes absorbed to the amorphous carbon support, parallel beam illumination was directed at the center of a presumably graphene oxide covered hole for 3 s, with the resulting diffraction pattern captured on the CCD detector.

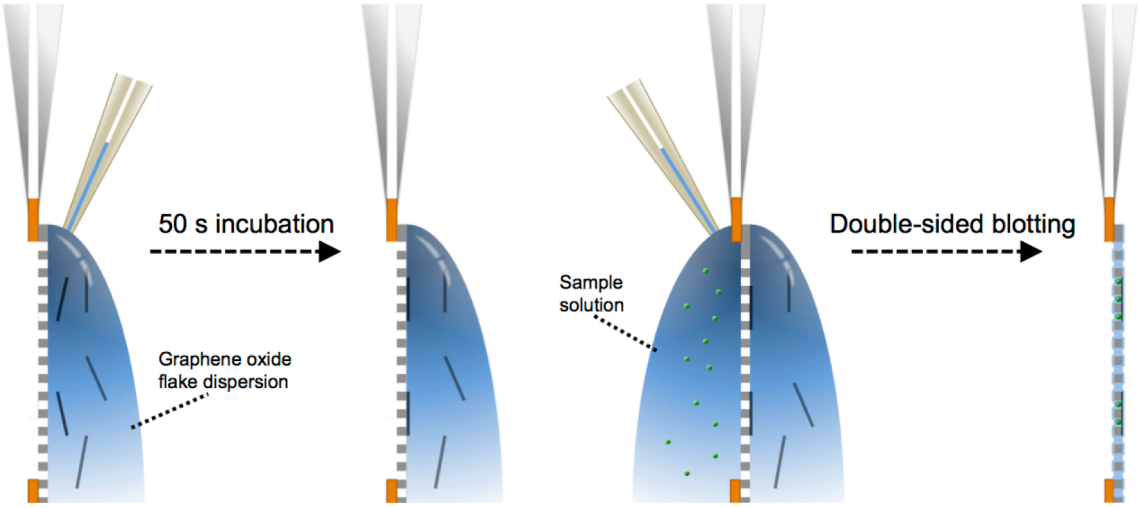

Figure 1. Key steps in the hydrated-graphene oxide process

A 3 µl drop of graphene oxide flake dispersion (diluted 1/10 in water from stock) is applied to the carbon side of a transmission electron microscopy grid and incubated for 50 s in saturating humidity (100%, 4 °C). During this period, graphene oxide flakes absorb to the amorphous carbon support. Following incubation, 3 µl of sample solution is applied to the opposite, non-carbon side of the grid. Double-sided blotting is commenced immediately (total graphene oxide flake dispersion incubation time ~60 s). This process causes graphene oxide flakes and sample particles to interact within the holes of the carbon support. Immediate plunge-freezing forms vitreous ice films with sample particles dispersed throughout.

4. Perpetually-hydrated GO flakes can be incorporated into a standard sample preparation regime via the hydrated-GO process

The hydrated-GO process is introduced in section 2 (Hydrated-graphene oxide process) and **Fig. 1**. The process begins with the application of a drop of GO flake dispersion to the carbon face of a hydrophilised transmission electron microscopy (TEM) grid. To minimize evaporation, the droplet is incubated with the grid for 50 s under saturating humidity (100% humidity, 4 °C), during which time GO flakes ostensibly adsorb to the amorphous carbon surface. After the incubation step, a drop of sample is applied to the opposite, non-carbon face of the grid followed by immediate commencement of double-sided blotting and plunge-freezing. This process results in vitrified flakes of solubilized GO distributed across the amorphous carbon support, the presence of which was confirmed by electron diffraction (**Fig. S3a-c**). Significantly, the hydrated-GO process can be conducted without the need for additional tools, devices or extraneous treatment steps above what would be necessary in a standard preparation repertoire, thus making it a cost-effective and easily adoptable method.

The precise details of the process itself can be adjusted to suit specific needs; for example, vitreous ice film thickness can be tailored by optimizing blotting force/time and the number of vitrified GO flakes can be adjusted by varying the concentration of the GO flake dispersion. However, for the purpose of comparability in this study, conditions were kept constant for all tests and samples. Blotting conditions were optimized with a bias towards achieving the thinnest vitreous ice films possible rather than for sufficient particle dispersion, which is typically aided by suitably thick ice films. While this was borne out of necessity due to the electron beam of 20 kV, it allowed us to investigate the performance of the hydrated-GO process in conditions not typically conducive to good particle dispersion thus representing ‘challenging’ scenarios. We envisage that the hydrated-GO process will

perform at least as well when blotting conditions are tailored more towards sufficient particle dispersion and not thin ice.

The GO flake preparation used in this study was supplied as dispersed monolayer GO flakes in water with an average flake size of 22 μm^2 in surface area (based on manufacturer specifications), allowing for substantial grid coverage per flake. Each grid produced by the hydrated-GO process was inspected at low-magnification (full grid view) and 20 kV in order to qualitatively assess GO flake coverage. As can be seen from example images **Fig. S3a** and **d**, the vast majority of grid squares showed angular and patchy variations in contrast indicative and consistent with the presence of GO flakes. However, due to natural size variations, folding, fragmentation and aggregation of GO flakes in solution (the last of which is reversible by sonication, according to the product specifications), the distribution of GO flakes across the grid surface showed distinct variability, with some squares containing only small fragments of GO flakes while GO agglomerates were present in others. While this made precise quantification of grid coverage difficult, most grid squares displayed significant GO flake coverage (approximately 50% coverage or greater) (**Fig. S3b,e**). Electron diffraction analyses of grid squares with significant expanses of GO coverage displayed Bragg diffraction patterns consistent with monolayer GO (**Fig. S3c**), although it must be noted that bilayer GO with carbon atoms stacked in exact alignment (AA stacking) or in a Bernal-stacked form (AB stacking) would also display similar Bragg diffraction patterns and would therefore not be distinguishable from monolayer GO by electron diffraction (Charlier et al., 1992; Guadagno et al., 2015; Lee et al., 2016). In our view, however, these precise stacking arrangements would not be the major forms given the imprecise nature of monolayer GO flake stacking in solution and inevitable 'twisting' between layers (Ramnani et al., 2017), which leads us to believe in a predominance of monolayer GO flakes (in targeted areas).

In general, we found the hydrated-GO process to be highly reproducible from grid to grid, with the ease of producing suitable grids no different to a conventional sample preparation regime. This is to be expected since the hydrated GO flakes are introduced into the sample preparation regime in a minimally intrusive manner. We believe this to be one of the key strengths of the proposed method since it would easily allow researchers to test the method with their samples.

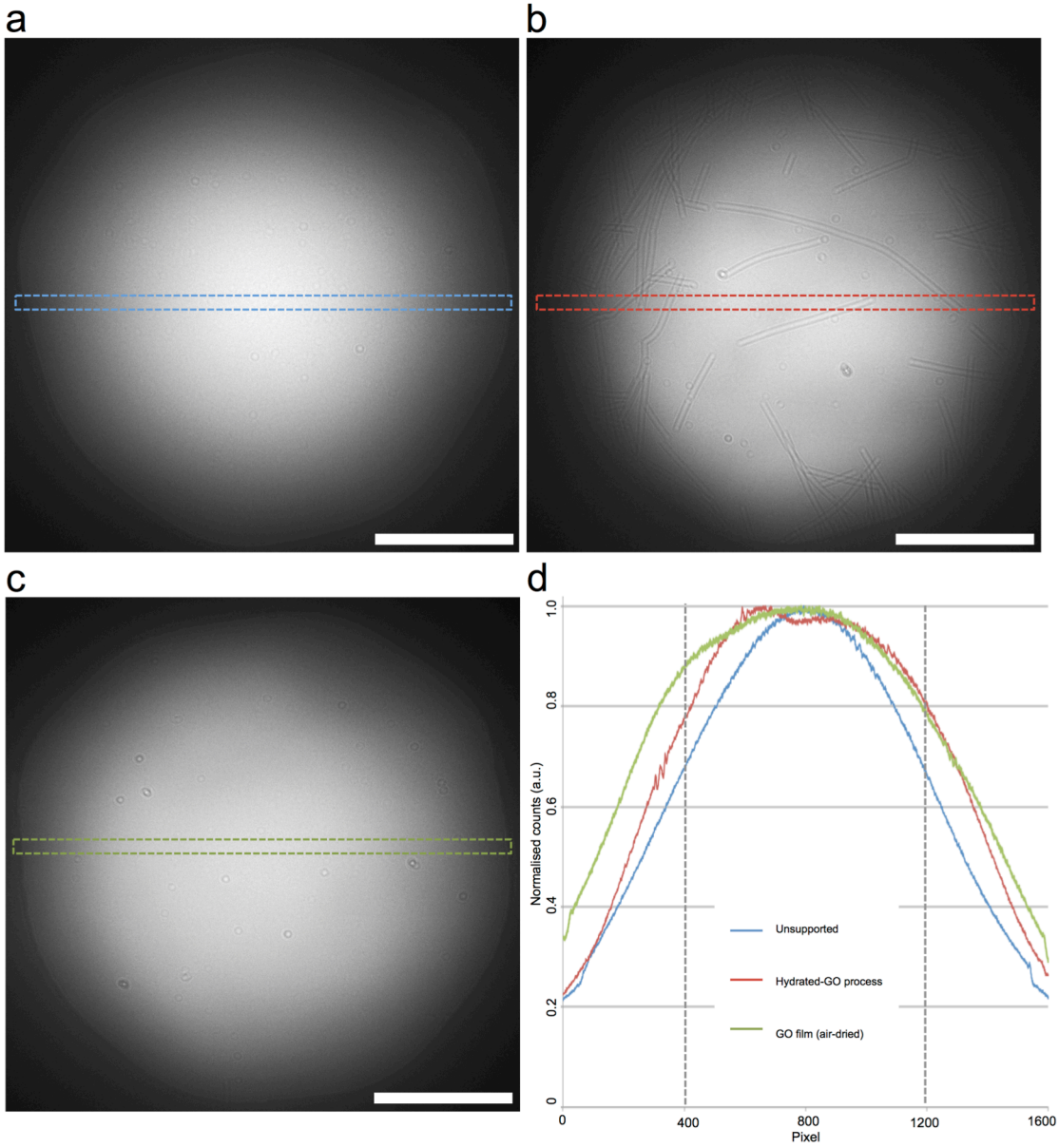

Figure 2. Perpetually-hydrated graphene oxide flakes in vitreous ice films improve sample particle dispersion

All images are acquired with strong defocus, low-kV TEM to provide strong particle contrast, as detailed in the main text. (**A-C**) Vitreous ice films of purified tobacco mosaic virus particles suspended within holes of amorphous carbon supports, prepared using (**A**) a conventional vitrification process (unsupported), (**B**) perpetually-hydrated graphene oxide flakes with the hydrated-graphene oxide process and (**C**) a graphene oxide film grid with an air-dried intermediate state. Isolated and dispersed tobacco mosaic virus particles were only observed with the sample prepared using the hydrated-graphene oxide process, as in (**B**). All scale bars, 1,000 nm. (**D**) Detector counts, normalized to peak counts, integrated down boxes in A-C (1,600 x 100 pixels) with respect to an unperturbed beam ($Intensity/Intensity_{max}$, **Fig. S5**). Wider plateaus in intensity from the hole centers to half radii distances (dotted lines) indicate more uniformly thick ice films in the presence of graphene oxide, with respect to the unsupported ice film..

5. Perpetually-hydrated GO flakes improve particle dispersion in cryo-EM

The effect of the hydrated-GO process on particle dispersion is demonstrated in **Fig. 2.** In this case, the dispersions of purified tobacco mosaic virus particles (TMV, ~34 MDa) were compared, following vitreous ice preparation with conventional (no GO, hereinafter termed 'unsupported' vitreous ice films), hydrated-GO, and air-dried GO processes, respectively. In the first case, rigorous inspection of the grid revealed an almost total absence of TMV particles from within the holes (**Fig. 2a**), as expected. In contrast, when the hydrated-GO process was employed (with same source TMV sample), considerable improvements in TMV particle density and dispersion were consistently observed (**Fig. 2b**). Furthermore, when a more traditional GO process, with intermediate air-dry stages, was employed, the appearance was similar to the unsupported ice film reference case (**Fig. 2c**). This is important as it clearly shows that it is the "perpetual-hydration", rather than just the presence of GO flakes, which is the decisive factor in improving particle dispersion. A further positive finding was that with the hydrated-GO process, isolated particles were observed even with substantially diluted TMV samples. This is contrary to the typical requirement in cryo-EM for highly concentrated samples in order to achieve sufficient particle density (**Note S1** and **Fig. S4**).

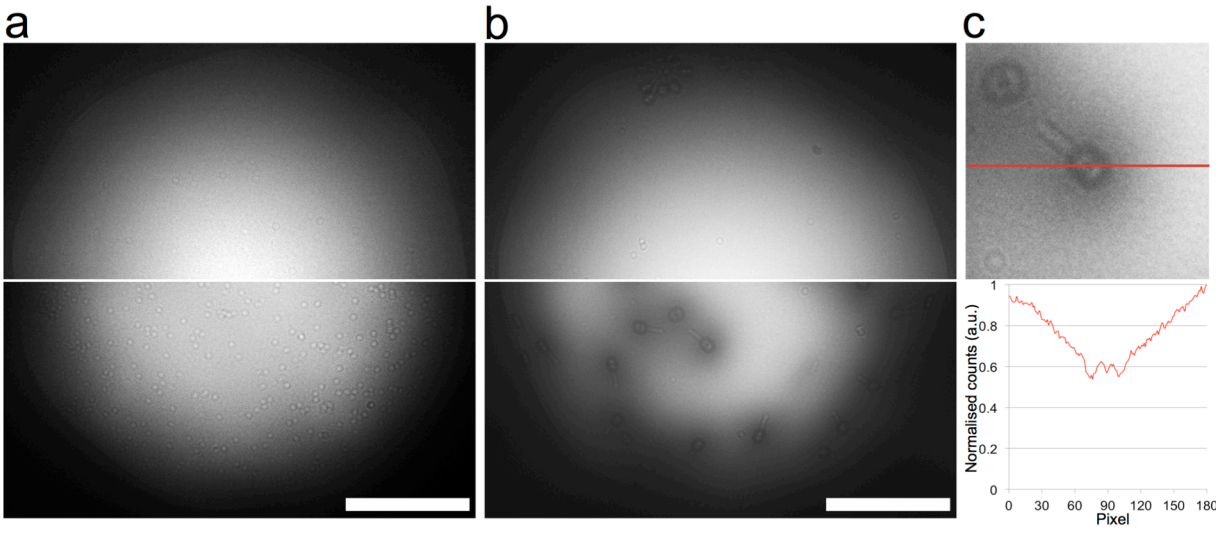

Figure 3. Improved dispersion in vitreous ice films of erythrocruorin and bacteriophage T4 with the graphene oxide-optimized process

(**A**,**B**) Cryo-electron microscope images of purified erythrocruorin (**A**) and bacteriophage T4 (**B**) in vitreous ice films prepared with a conventional vitrification process (top) and the graphene oxide-optimized process (bottom), showing vast improvements in particle dispersion in the presence of graphene oxide. All scale bars, 1,000 nm. (**C**) High-magnification view of ice-embedded T4 particle adsorbed to graphene oxide (top), with corresponding peak count-normalized profile along the red line (bottom). Reduced beam intensity at the particle, with respect to surrounding areas void of particles, suggests thicker ice in this region.

To assess the effect of GO on the shape of vitreous ice films, normalized beam intensity profiles, after correction for the unperturbed beam profile (Fig. S5), were compared. With the conventional vitrification process, the unsupported ice film biconcavity resulted in gradual decreases in intensity from the center holes to the periphery. In both cases where GO was present, wider plateaus of uniform intensity were detected at the centers of the holes, indicating reduced biconcavity and more uniformly thick ice films in the presence of GO (Fig. 2d). Thus, while both the hydrated-GO process and air-dried GO film grid result in better thickness uniformity, only the hydrated-GO process accomplishes this in tandem with improved specimen dispersion.

6. Sample and GO flake incompatibility issues are avoided through a double-sided application and blotting scheme

The double-sided application and blotting approach, as detailed in **Fig. 1**, was identified as a critical component in this process, owing to problems with specimen and/or GO flake aggregation. For example, when the GO flake dispersion and a sample of purified erythrocruorin (~3.6 MDa) were mixed, considerable and near instantaneous aggregation of GO was observed (**Fig. S6**). By partitioning the two solutions with the grid, brief mixing is primarily restricted to the blotting phase of the process and through the holes of the amorphous carbon support. This temporal and spatial segregation scheme minimized GO aggregation and resulted in a marked improvement in erythrocruorin dispersion (**Fig. 3a**). As samples can essentially be used as-purified (albeit at optimized concentrations), this should vastly broaden the potential applicability of the hydrated-GO process.

7. Vitreous ice film thickness conforms to GO adsorbed particles through a self-regulatory mechanism

The hydrated-GO process was also tested on enterobacteriophage T4 (~195 MDa). This is a challenging specimen that typically resists uniform dispersion in prohibitively thin ice films due to the large dimensions (1195 x 860 Å) of its icosahedral head structure (Fokine et al., 2004). Without needing to change blotting conditions (conditions where kept constant throughout all tests in this study) to create thicker, more accommodating vitreous ice films, good particle dispersion was successfully achieved with the hydrated-GO process (**Fig. 3b**). Interestingly, regions of gradually-reducing beam intensity were observed centered at the GO-adsorbed T4 particles (**Fig. 3c**), which suggests locally thicker ice in these regions. We hypothesize that the vitreous ice conforms to the GO-absorbed particles, possibly due to these particles retaining an encompassing shell of liquid when the majority is removed during blotting (**Fig. S7**). This self-regulatory mechanism of ice thickness would be highly beneficial in avoiding unnecessarily thick ice films.

8. Conclusions

As cryo-EM has developed into an indispensible tool in structural biology, the further widespread application to various macromolecules will be partly governed by the ability to successfully disperse particles in vitreous ice films. In this study, we've demonstrated that multiple sample preparation benefits of GO can be exploited by maintaining constant hydration. The hydrated-GO process successfully integrates GO into a conventional sample preparation regime without the need for additional tools or devices, making it a cost-effective and easily adoptable method. Although the use of graphene and GO films in cryo-

EM is well documented, we found the hydrated-GO process to perform significantly better than conventional air-dried GO film grids with regard to increasing particle dispersion. Furthermore, whereas graphene, GO and thin carbon substrates often require significant preparatory periods for grid fabrication and/or cleaning (if commercially available grids are used), the hydrated-GO process essentially fabricates a hydrophilic GO film grid during the blotting phase thereby only adding an additional incubation step of ~60 s to the total sample preparation regime, making it a highly efficient method.

In this study, we've refrained from making direct claims regarding the effect of the hydrated-GO process on achievable structural resolution. We cannot rule out the possibility that for certain specimens, for example, where preferential orientations are adopted upon binding to the GO flakes, structural resolution may be hindered by the presence of GO. However, it is evident from this study that for specimens where poor dispersion completely precludes analysis by cryo-EM, the hydrated-GO process should be advantageous since it will, at the very least, allow for some degree of structural analysis to occur. We believe that the hydrated-GO process will be most beneficial when applied to such samples. It should also be noted that the ability to successfully disperse particles in vitreous ice films has uses beyond single-particle and tomographic cryo-EM approach. For example, the emerging field of individual/single molecule imaging could benefit from the hydrated-GO process since these imaging methods do not require a large particle data set but would instead be dependent on vitreous ice film thickness, concomitant with the low-energy beams used (Stevens et al., 2011, Longchamp et al., 2017, Adaniya et al., 2018). Being able to image particles near the centers of grid holes, where vitreous ice films are typically thinnest, would be highly advantageous for such imaging schemes.

The true widespread effectiveness of the hydrated-GO process, in improving sample dispersion and achievable structural resolution, requires further investigation on a case-by-case basis. Nevertheless, the significant improvements seen for the specimens in this study are promising signs indeed and will hopefully engender further investigations into the use of perpetually-hydrated GO flakes in cryo-EM.

ACKNOWLEDGEMENTS

We would like to thank Dr. Ryusuke Kuwahara (Okinawa Institute of Science and Technology Graduate University, Japan) for discussions regarding cryo-EM and associated methodologies; Prof. Keiichi Namba, Dr. Takayuki Kato, Dr. Tomoko Miyata and Ms. Naoko Kajimura (Osaka University, Japan) for initial TMV samples and discussions regarding graphene. **Funding:** The Quantum Wave Microscopy Unit is supported by funds from the Okinawa Institute of Science and Technology Graduate University, Japan.

AUTHOR CONTRIBUTIONS

M.C, H.A., and T.S. conceptualized the method and validation experiments. M.C., H.A., and C.C. processed data. M.Y., K. L., S.T., M.C., and H.A. prepared samples for visualization.

DECLARATION OF INTERESTS

The authors declare no competing interests.

REFERENCES

Adaniya, H., Cheung, M., Cassidy, C., Yamashita, M., Shintake, T. (2018). Development of a SEM based low-energy in-line electron holography microscope for individual particle imaging. Ultramicroscopy *188*, 31-40

Arnold, S.A., Albiez, S., Bieri, A., Syntychaki, A., Adaixo, R., McLeod, R.A., Goldie, K.N., Stahlberg, H., Braun, T. (2016). Blotting-free and lossless cryo-electron microscopy grid preparation from nanoliter-sized protein samples and single-cell extracts. J. Struct. Biol. *197,* 220-226.

Burrows, N. and Penn, R.L. (2013). Cryogenic transmission electron microscopy: aqueous suspensions of nanoscale objects. Microsc. Microanal. *19*, 1542-1553.

Charlier, J.C. and Michenaud, J.P. (1992-II). First-principles study of the electronic properties of simple hexagonal graphite. Phys. Rev. B *46* (8), 4531-4539

Cheung, M., Kajimura, N., Makino, F., Ashihara, M., Miyata, T., Kato, T., Blocker, A.J. (2013). A method to achieve homogeneous dispersion of large transmembrane complexes within the holes of carbon films for electron cryomicroscopy. J. Struct. Biol. *182*, 51-56..

Dubochet, J., Adrian, M., Chang, J.J., Homo, J.C., Lepault, J., McDowall, A.W., Schultz, P. (1988). Cryo-electron microscopy of vitrified specimens. Q. Rev. Biophys. *21*, 129-228

Dubochet, J., Groom M., Mueller-Neuteboom, S. (1982). Adv, Opt. Electron Microsc. *8*, 107-135.

Fokine, A., Chipman, P.R., Leiman, P.G., Mesyanzhinov, V.V., Rao, V.B., Rossmann, M.G. (2004). Molecular architecture of the prolate head of bacteriophage T4. Proc. Natl. Acad. Sci. *101,* 6003-6008.

Frank, J. Three-dimensional electron microscopy of macromolecular assemblies: visualization of biological molecules in their native state 2nd edition. (2006). New York, Oxford University Press.

Guadagno, L., Sarno, M., Vietri, U., Raimondo, M., Cirillo, C., Ciambelli, P. (2015) Graphene-based structural adhesive to enhance adhesion performance. RSC Adv. *5*, 27874-27886

Lee, J. K., Kim, J-G., Hembram, K. P. S. S., Kim, Y-I., Min, B-K., Park, Y., Lee, Y.K., Moon, D.J., Lee, W., Lee, S.G., John, P. (2016). The Nature of Metastable AA′ Graphite: Low Dimensional Nano- and Single-Crystalline Forms. Sci. Reports *6*, 39624

Loh, K.P., Bao, Q., Eda G., Chhowalla, M. (2011). Graphene oxide as a chemically tunable platform for optical applications. Nat. Chem. *2*, 1015-1024.

Longchamp, J.N., Latychevskaia T., Escher, C., Fink, H.W. (2015). Low-energy electron holographic imaging of individual tobacco mosaic virions. Appl. Phys. Lett. *107*, 133101

Lu, Z., Shaikh, T.R., Barnard, D., Meng, X., Mohamed, H., Yassin, A., Mannella, C.A., Agrawal, R.K., Lu, T.M., Wagenknecht, T. (2009). Monolithic microfluidic mixing-spraying devices for time-resolved cryo-electron microscopy. J. Struct. Biol. *168,* 388-398.

Meyerson, J.R., Rao, P., Kumar, J., Chittori, S., Banerjee, S., Pierson, J., Mayer, M.L., Subramaniam, S. (2014). Self-assembled monolayers improve protein distribution on holey carbon cryo-EM supports. Sci. Reports *4*, 7084.

Neklyudov, V.V., Khafizov, N.R., Sedov, I.A., Dimiev, A.M. (2017). New insights into the solubility of graphene oxide in water and alcohols. Phys. Chem. Chem. Phys. *19*, 17000-17008.

Orlova, E.V., and Saibil, H.R. (2011). Structural analysis of macromolecular assemblies by electron microscopy. Chem. Rev. *111*, 7710–7748.

Pantelic, R.S., Meyer, J.C., Kaiser, U., Baumeister W., Plitzko, J.M. (2010). Graphene oxide: a substrate for optimizing preparations of frozen-hydrated samples. J. Struct. Biol. *170,* 152-156.

Pantelic, R.S., Suk, J.W., Hao, Y., Ruoff R.S., Stahlberg, H. (2011). Oxidative doping renders graphene hydrophilic, facilitating its use as a support in biological TEM. Nano Lett. *11,* 4319-4323.

Paredes, J.I., Villar-Rodil, S., Martinez-Alonso, A., Tascón, J.M.D. (2008). Graphene oxide dispersions in organic solvents. Langmuir. *24*, 10560-10564.

Patterson, J.P., Sanchez, A.M., Petzetakis, N., Smart, T.P., Epps, T.H. 3rd, Portman, I., Wilson, N.R., O'Reilly, R.K. (2012). A simple approach to characterizing block copolymer assemblies: graphene oxide supports for high contrast multi-technique imaging. Soft Matter *8* (12), 3322-3328.

Pankaj Ramnani, Mahesh R. Neupane, Supeng Ge, Alexander A. Balandin, Roger K. Lake, Ashok Mulchandani (2017). Raman spectra of twisted CVD bilayer graphene. Carbon *123*, 302-306

Razinkov, I., Dandey, V., Wei, H., Zhang, Z., Melnekoff, D., Rice, W.J., Wigge, C., Potter, C.S., Carragher, B. (2016). A new method for vitrifying samples for cryoEM. J. Struct. Biol. *195,* 190-198.

Rhinow, D., Büenfeld, M., Weber, N.E., Beyer, A., Gölzhäuser, A., Kühlbrandt, W., Hampp, N., Turchanin, A. (2011). Energy-filtered transmission electron microscopy of biological samples on highly transparent carbon nanomembranes. Ultramicroscopy *111,* 342-349.

Russo, J.R. and Passmore, L.A. (2014). Controlling protein adsorption on graphene for cryo-EM using low-energy hydrogen plasmas. Nat. Methods. *11*, 649-652.

Snijder, J., Borst, A.J., Dosey, A., Walls, A.C., Burrell, A., Reddy, V.S., Kollman, J.M., Veesler, D. (2017).Vitrification after multiple rounds of sample application and blotting improves particle density on cryo-electron microscopy grids. J. Struct. Biol. *198*, 38-42.

Steven, A., Baumeister, W., Johnson, L., Perham, R. (2016). Molecular Biology of Assemblies and Machines, (Garland Science, First edition)

Stevens, G.B., Krüger, M., Latychevskaia, T., Lindner, P., Plückthun, A., Fink., H.W. (2011). Individual filamentous phage imaged by electron holography. Eur. Biophys. J. *40*, 1197

van de Put, M.W., Patterson, J.P., Bomans, P.H., Wilson, N.R., Friedrich, H., van Benthem, R.A., de With, G., O'Reilly, R.K., Sommerdijk, N.A. (2015). Graphene oxide single sheets as substrates for high resolution cryoTEM. Soft Matter *11*, 1265-1270.

Yuan, B., Zhang Z., Zhou, K. (2011). Graphene oxide monolayers as supporting films for high resolution transmission electron microscopy. Appl. Surf. Sci. *257*, 5754-5758.

SUPPLEMENTAL INFORMATION

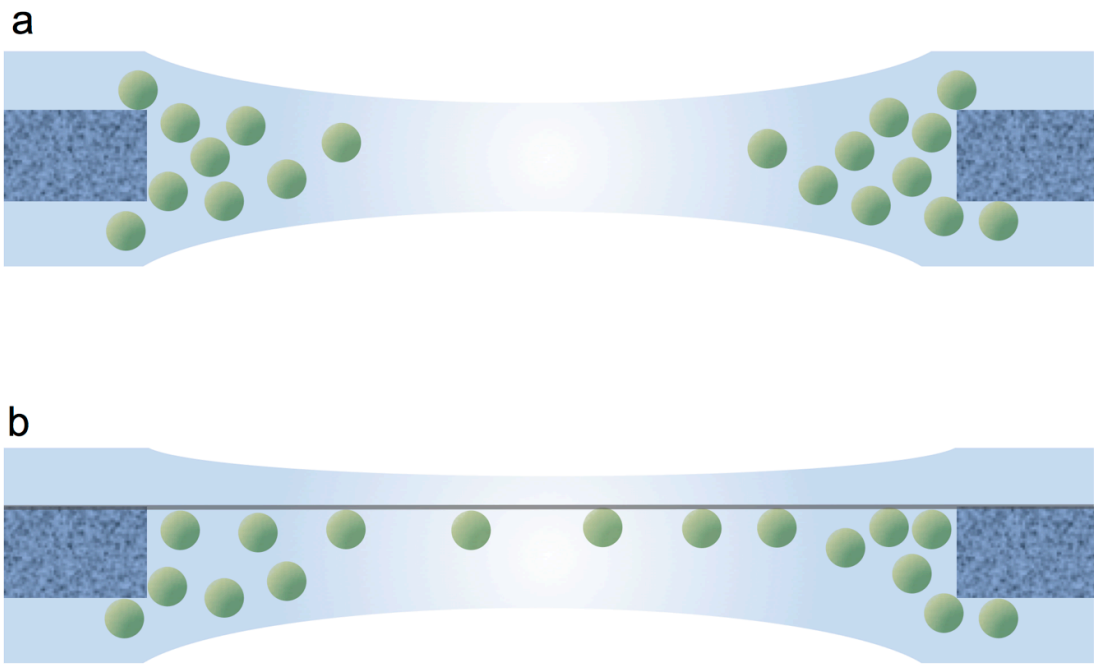

Figure S1. Particle dispersion in vitreous ice films within holes of an amorphous carbon support

(**A**) Nanometer-thick unsupported vitreous ice films are biconcave in nature, causing particles in solution to agglomerate at the peripheries of holes. Non-covalent, covalent and/or ionic interactions between specimen particles and the amorphous carbon further prevent uniform dispersion of particles. (**B**) Thin carbon films, such as graphene oxide, mounted atop the amorphous carbon support can promote particle dispersion by providing a surface for particles to adsorb to during sample preparation.

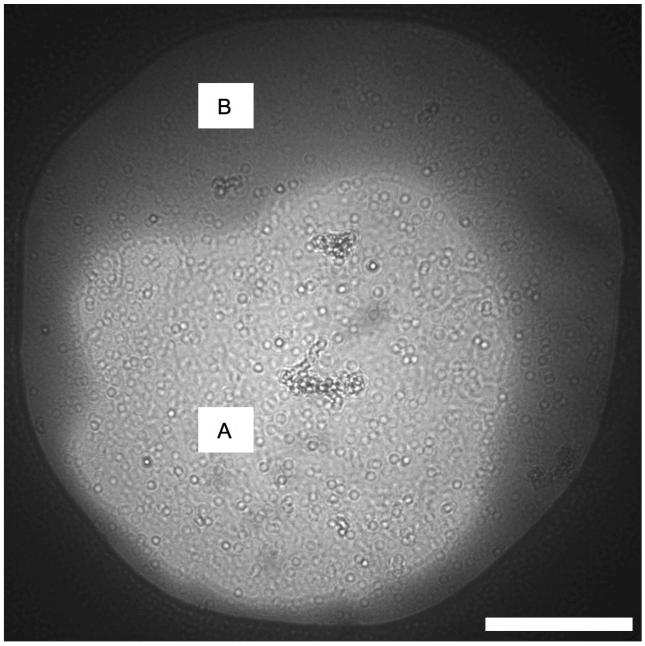

Figure S2. Dewetting of air-dried graphene oxide films during sample preparation causes vitreous ice film discontinuity
The above image shows a cryo-electron microscope micrograph of a vitreous ice film of distilled water, prepared using an air-dried graphene oxide film grid. The hydrophobic nature of dehydrated graphene oxide causes surface dewetting during sample preparation, manifesting as local ice-free pockets in vitreous ice films. Such a localized ice-free pocket is shown here, with the region of increased beam intensity (A) indicating the absence of vitreous ice from the graphene oxide surface, surrounded by darker regions of vitreous ice (B). Scale bar, 1,000 nm.

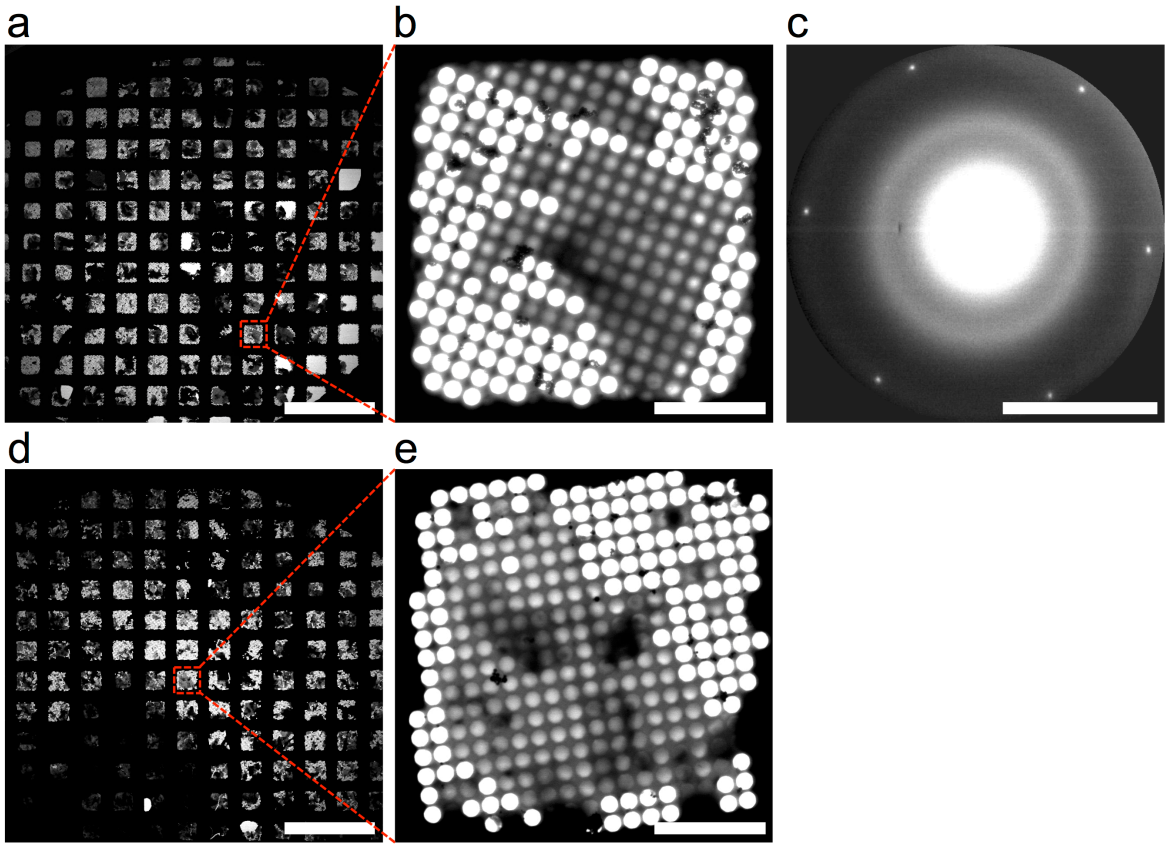

Figure S3. Hydrated-graphene oxide process sample preparation results in vitrified graphene oxide flake adsorption to the amorphous carbon support

(**A,D**) Low magnification STEM image of a grid following hydrated-graphene oxide process sample preparation, showing areas of contrast variation within a large number of grid squares. Scale bar, 500 µm. (**B,E**) STEM image of an individual grid square reveals the possible presence of adsorbed graphene oxide flakes. Scale bar, 30 µm. (**C**) Low-energy (20 kV) electron diffraction acquired from a covered hole shows the characteristic six first order Bragg diffraction spots of graphene oxide, confirming the successful adsorption of graphene oxide flakes to the amorphous carbon support. Scale bar, 5 nm^{-1}.

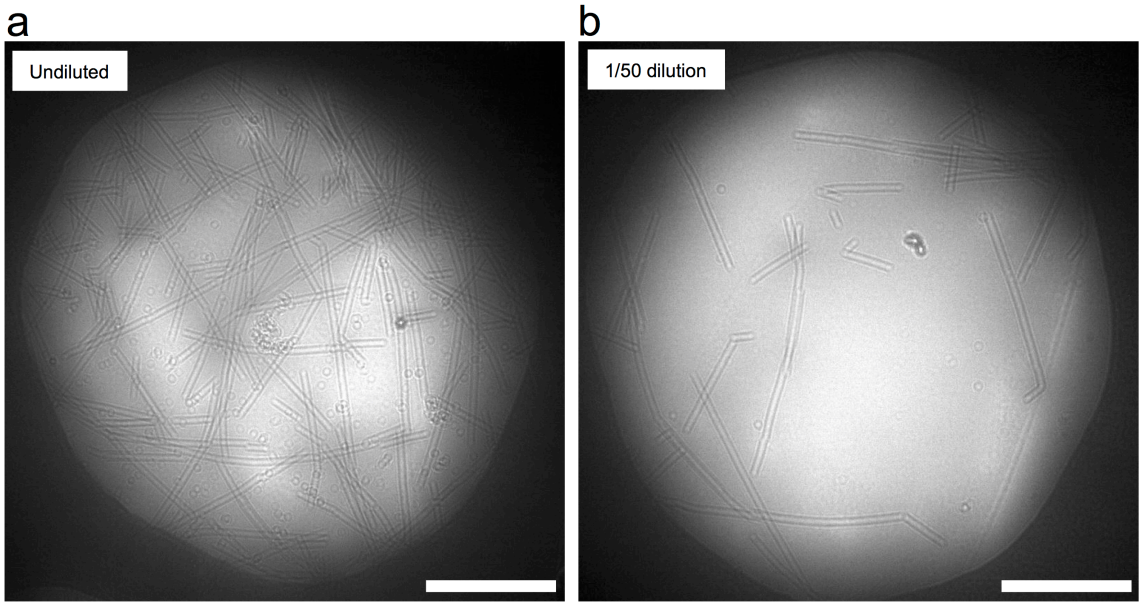

Figure S4. With the hydrated-graphene oxide process, even with relatively low sample concentrations the dispersion of particles in the suspended vitreous ice is adequate

(**A**) Cryo-electron microscopy image of tobacco mosaic virus particles dispersed in a vitreous ice film suspended within the hole of an amorphous carbon support, prepared using an undiluted tobacco mosaic virus sample (concentration ~ 5.5 mg/ml) and the hydrated-graphene oxide process. Tobacco mosaic virus particles are dispersed in the hole at a high density. (**B**) Hydrated-graphene oxide process applied to the sample after 1/50 dilution in distilled water (concentration ~ 0.1 mg/ml). Particles can still be observed near the center of the hole (refer to **Note S1**). All scale bars, 1,000 nm.

Note S1. Number of vitreous ice film-embedded tobacco mosaic virus (TMV) particles per hole of an amorphous carbon support after sample preparation

In order to assess the dependence of particle density and dispersion on sample concentration, the number of expected TMV particles per hole was calculated as follows:

Sample: Purified TMV (average length, 300 μm; molecular weight, ~ 36 MDa) (Steven et al., 2016) solution with a measured protein concentration of 0.1 mg/ml (1/50 diluted sample, **Fig. S4b**)

Grid: Quantifoil 3.5/1 (3.5 μm diameter holes)

Assuming a homogenous dispersion of TMV particles in the sample solution:

Moles of TMV per μl = $\frac{0.0001\ (g)}{36{,}000{,}000\ (Da)} \times \frac{1}{1000}$

= 2.8×10^{-15} mol/μl

Assuming a continuous vitreous ice film thickness of 0.1 μm (conservative estimate):

Volume of ice in grid hole = $\pi \times 1.75^2 \times 0.1$

= $0.96\ \mu m^3$

Volume of solution per hole = $0.96\ (\mu m^3) \times 1 \times 10^{-9}$

= 9.6×10^{-10} μl

Moles of TMV per hole = 2.8×10^{-15} (mol/μl) x 9.6×10^{-10} (μl)

= 2.7×10^{-24} mol

TMV particles per hole = 2.7×10^{-24} (mol) x 6.02×10^{23} (Avogadro's constant)

= 1.6 or **1-2 particles per hole**

Even with a conservative vitreous ice film thickness estimate of 100 nm, the number of TMV particles per hole seen after sample preparation with the hydrated-GO process exceeds expectation (**Fig. S4b**). Based on data not included in this study, we estimate the thickness of vitreous ice films using the hydrated-GO process to be between 30 - 50 nm for TMV, which would reduce this figure to 1 particle per hole or fewer.

Observations with TMV would therefore indicate that the use of GO in the hydrated-GO process enhances particle density and dispersion within holes of amorphous carbon supports beyond what would be possible using a conventional vitrification process.

Since a protein concentration of 0.1 mg/ml for a ~36 MDa specimen is regarded as low for cryo-EM, this suggests that the hydrated-GO process can avoid, to some degree, the typical requirement for highly concentrated samples to achieve satisfactory particle density and dispersion in vitreous ice films.

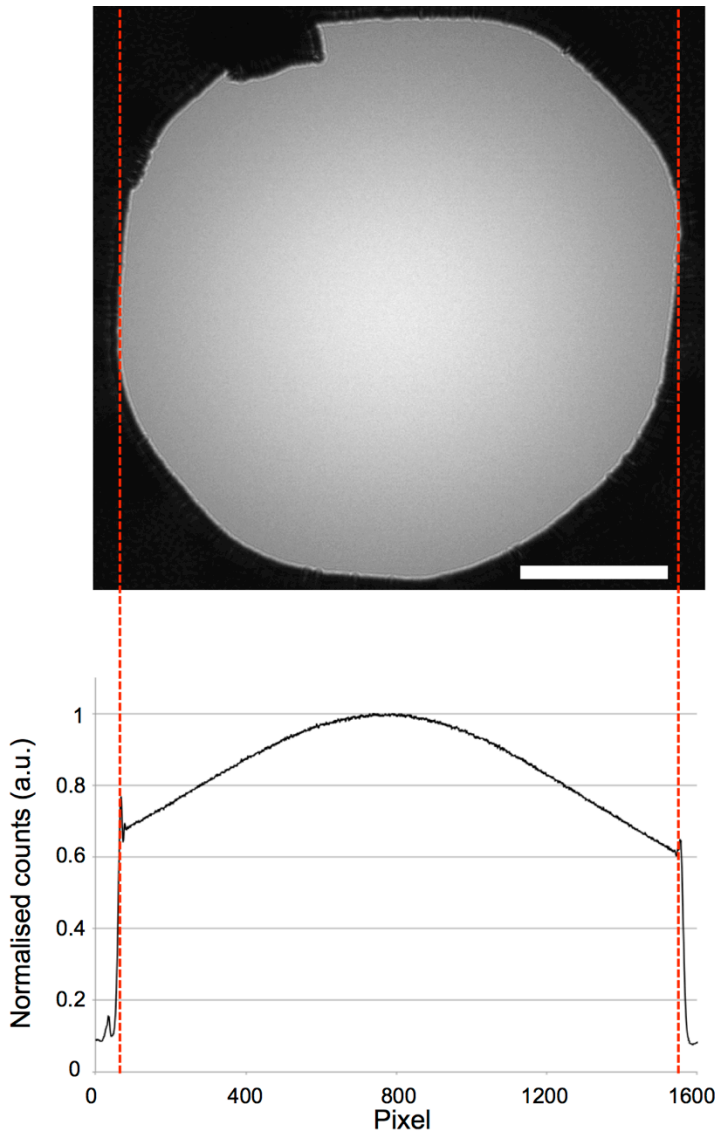

Figure S5. Profile of normalized detector counts of unperturbed electron beam

20 kV electron beam illumination through an empty 3.5 μm hole of a Quantifoil 3.5/1 grid for 500 ms. Scale bar, 1,000 nm.

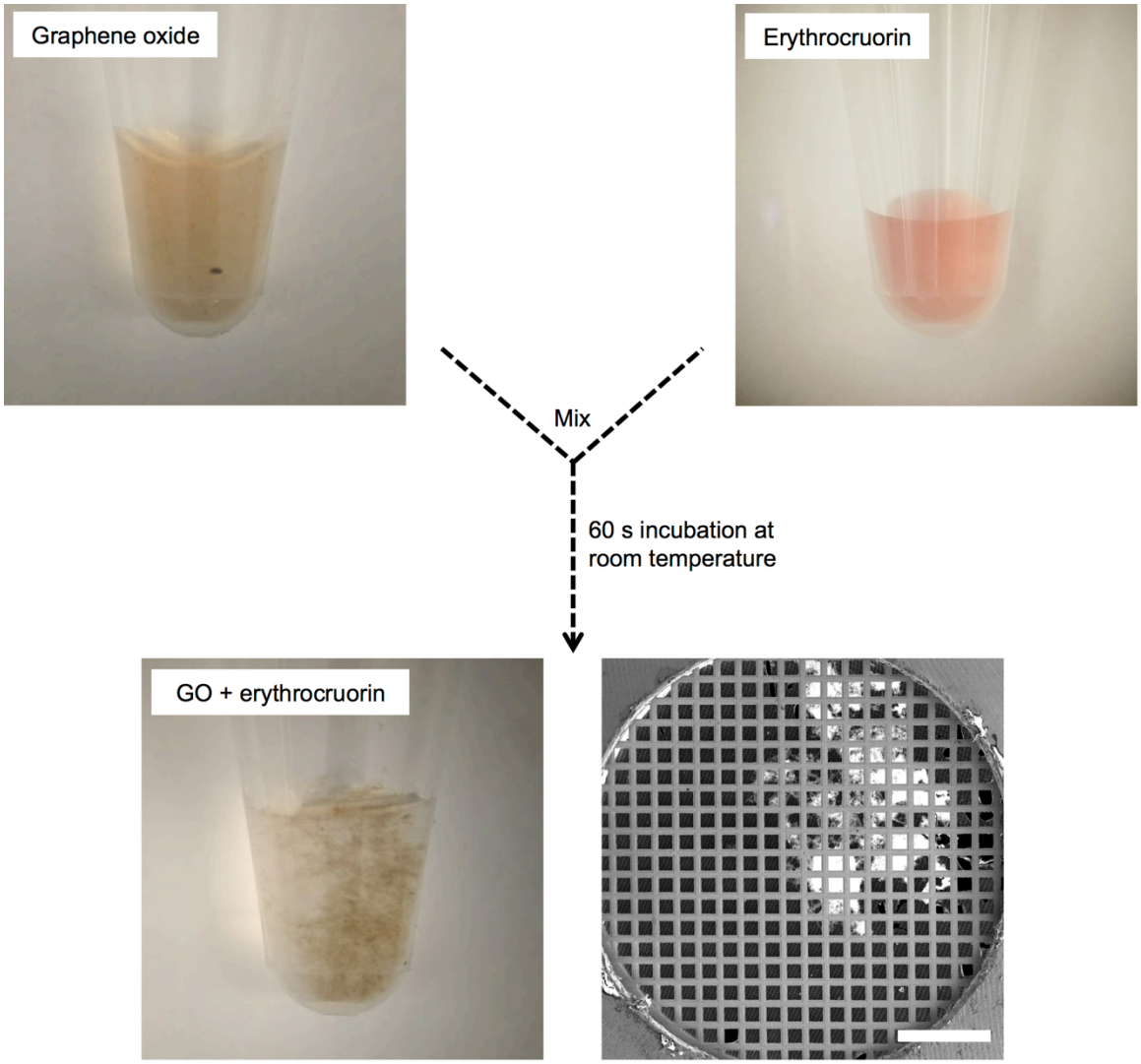

Figure S6. Solution incompatibility causes graphene oxide flake aggregation

Mixing of a solution of graphene oxide flake dispersion and purified erythrocruorin, at a volumetric ratio of 100:1, causes near-instantaneous aggregation of graphene oxide, as reflected by the loss of graphene oxide flake dispersion homogeneity after 60 s incubation at room temperature. Scanning electron microscopy evaluation of the graphene oxide flake dispersion + erythrocruorin mixture reveals large graphene oxide aggregates (white area) and the absence of solubilized graphene oxide flakes. Scale bar, 500 μm.

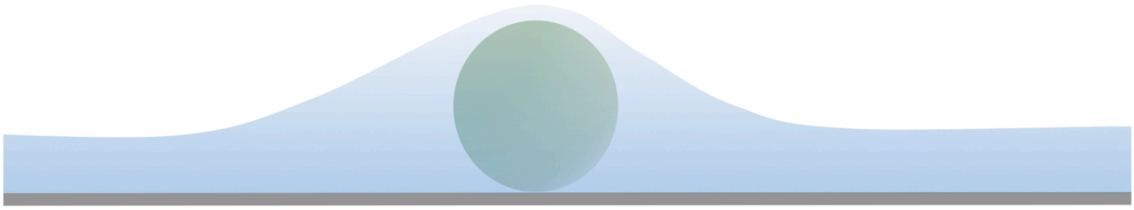

Figure S7. Hypothetical model of vitreous ice film surface topology conforming to a particle absorbed to graphene oxide
With the hydrated-graphene oxide process, particles adsorbed to the graphene oxide surface retain an encompassing shell of solution during blotting, resulting in increased ice thickness around the particle, with respect to areas void of particles. Ice thickness around adsorbed particles is therefore regulated by the dimensions of the particles.